

## **Fast and Accurate Thermal Modeling of Magnetic Components by FEA-Based Homogenization**

G. Salinas López, A. D. Expósito, J. Muñoz-Antón, J. Á. O. Ramírez and R. P. López

### **► To cite this version:**

G. Salinas López, A. D. Expósito, J. Muñoz-Antón, J. Á. O. Ramírez and R. P. López, "Fast and Accurate Thermal Modeling of Magnetic Components by FEA-Based Homogenization," in IEEE Transactions on Power Electronics, vol. 35, no. 2, pp. 1830-1844, Feb. 2020, doi: 10.1109/TPEL.2019.2921160.

### **Published version.**

Published February 2020

**Archivo Digital UPM** houses in digital format the academic and scientific documentation (theses, pfc, articles, etc.) generated at the institution and makes it accessible through the Internet, within the framework of the Budapest Open Access Initiative and the Berlin Declaration, of which the Universidad Politécnica de Madrid is a signatory.

El **Archivo Digital UPM** alberga en formato digital la documentación académica y científica (tesis, pfc, artículos, etc.) generada en la institución, y la hace accesible a través de Internet, en el marco de la Iniciativa por el Acceso Abierto de Budapest y la Declaración de Berlín, de la que es signataria la Universidad Politécnica de Madrid.

# Fast and Accurate Thermal Modeling of Magnetic Components by FEA-based homogenization

Guillermo Salinas López\* , Alberto Delgado Expósito\* , Javier Muñoz-Antón† ,  
Jesús A. Oliver Ramírez\* , Roberto Prieto López\* 

\*Centro de Electrónica Industrial, Universidad Politécnica de Madrid, Madrid, Spain

†Grupo de Investigaciones Termoenergéticas, Universidad Politécnica de Madrid, Madrid, Spain

Contact: [guillermo.salinas@upm.es](mailto:guillermo.salinas@upm.es), +34 616 633 787

**Abstract**—The use of 3D thermal simulations of magnetic components for power converters is limited to validation of final designs due to time consumption. A two-step homogenization is proposed to simplify them, while keeping good accuracy. The required equations and some guidelines are described in this paper. It can be applied to solid round wire, litz wire or foil wound magnetic components. Considerations to extend its use to transformers, including the use of interleaving techniques and insulating tape are explained. This method can reduce the computation time of 3D simulations (seven times faster than usual simulations) while the convergence is assured even for complex structures or cases with litz wire. Finally, the method is experimentally validated with DC and AC excitation.<sup>1</sup>

**Keywords**—electrothermal effects, power transformer thermal factors, inductors, transformers

## NOMENCLATURE

$a, b, c, d$	Coefficients for the proposed multivariable fitting.
$A_{cond}$	Area of conductor.
$A_{ins}$	Area of insulation.
$AWG$	American Wire Gauge.
$h$	Heat transfer coefficient or film coefficient.
$k$	Thermal conductivity.
$k_a$	Thermal conductivity of surrounding material (air, potting).
$k_{bund}$	Thermal conductivity of a litz bundle.
$k_{cond}$	Thermal conductivity of conductor material.
$k_{eq}$	Effective thermal conductivity.
$k_{eqort}$	Effective thermal conductivity in the orthogonal direction.
$k_{eqr}$	Effective thermal conductivity in the radial direction.
$k_{eq\theta}$	Effective thermal conductivity in the angular direction.
$k_{eqtan}$	Effective thermal conductivity in the tangential direction.
$k_{eqTOT}$	Effective thermal conductivity of several homogenized blocks.
$k_{eqz}$	Effective thermal conductivity in the vertical direction.
$k_{fe}$	Thermal conductivity of ferrite.
$k_i$	Thermal conductivity of wire insulation.
$k'_i$	Homogenized thermal conductivity of different insulation.
$k_{ibund}$	Thermal conductivity of bundle impregnation.
$k_{imp}$	Thermal conductivity of wire impregnation.
$k_{ist}$	Thermal conductivity of strand insulation.
$k_{ins}$	Thermal conductivity of insulation layers.
$k_{ratio}$	Thermal conductivity ratio ( $k_w/k_a$ ).
$k_w$	Thermal conductivity of a homogenized wire.
$l_{cond}$	Width of conductors.
$l_{ins}$	Width of insulation layers.
$n_{cond}$	Number of conductor layers.
$n_{ins}$	Number of insulation layers.
$N_{layers}$	Total number of layers.
$PF$	Packing factor of a litz bundle.
$P_{pri}$	Losses in primary winding.

$P_{sec}$	Losses in secondary winding.
$q''$	Heat flux.
$q''_x$	Heat flux in the $x$ direction.
$r_1$	Inner radius of a cylindrical foil winding.
$r_n$	Radius of the $n$ foil layer.
$r_{crit}$	Critical radius.
$\tau$	Volume fraction of conductor material.
$\tau^*$	Introduced variable to replace $\tau$ .
$T_{cmax}$	Maximum core temperature.
$T_{c surf}$	Average core surface temperature.
$T_{wmax}$	Maximum winding temperature.
$T_{w surf}$	Average winding surface temperature.
$\Delta T$	Temperature rise.
$\Delta T_{exp}$	Measured temperature rise.
$\Delta T_{wireFEA}$	Temperature rise with 'wire level' homogenization.
$\Delta T_{sim}$	Temperature rise obtained by simulation.
$\Delta T_{windFEA}$	Temperature rise with 'winding level' homogenization.
$\phi$	Wire diameter.
$v_{cond}$	Volume of conductor material.
$v_{ist}$	Volume of strand insulation material.
$v_{imp}$	Volume of impregnation material.
$v_{ibund}$	Volume of bundle insulation.
$v_w$	Volume of a wire.
$w$	Width of the cell under study.

## I. INTRODUCTION

**D**ue to the interdependence between electromagnetic and thermal fields, proper modeling of both domains is needed to optimize magnetic components for power converters. As a result, a good accuracy of the thermal models is required to get better optimized magnetic components, with higher power density and lower size, while ensuring their operation below the thermal limit.

Some analytic solutions to estimate the temperature of the magnetic components can be found in the literature. Manufacturers usually provide empirical equations for each core shape [1], [2]. A simple equation was introduced in [3] for any core shape and size. These approaches are useful as first order approximations during the early design iterations, but its use in optimization processes would lead to non-optimized designs. Another empirical model for potted litz wound toroid inductors is developed in [4], while it offers a good accuracy, its use is limited to the shape of the component, the winding arrangement and the boundary conditions (no convection, since that model is developed for space environment conditions) used in their experimental setup.

Another approach to solve the thermal problem is the use of 1D models thermal networks. In [5], a one-dimensional thermal network is proposed to consider the heat transfer path from the center core leg of a magnetic component to the top

<sup>1</sup>This manuscript is an extension of the paper 'Fast FEA Thermal Simulation of Magnetic Components by Winding Equivalent Layers', presented in the recent ECCE'2018 conference, celebrated from 23th to 27th September 2018 at Portland (Oregon).

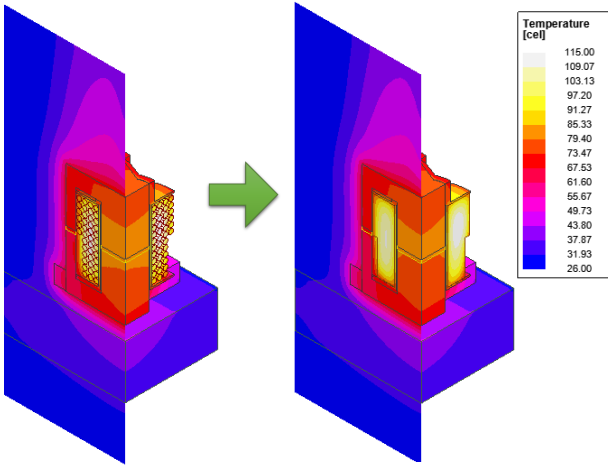


Fig. 1. 3D Thermal distribution on a cut plane of a PQ core inductor: detailed FEA simulation (left); homogenized winding (right).

and bottom core parts by means of parallel thermal resistors. The effect of convection and radiation inside the window is also modeled in [6]. Some details are added compared to [5] and avoid simplifying the radiation, but the heat transfer in other directions is neglected, what might infer a high error in the temperature estimation.

The most accurate solutions are achieved by means of 3D FEA simulations. The downside is that they are substantially time-consuming, due to the mesh requirements of the conductors, specially in the case of litz wires. Additionally, if the mesh is too demanding, like detailed simulations of litz wire windings, 3D simulations might become unfeasible.

Homogenization techniques have been traditionally used to simplify either the mathematical analysis or the simulations in different physics fields, which consist in replacing heterogeneous systems by a single component whose calculated properties make it macroscopically behave as the original system. In thermal analysis, that property is the effective thermal conductivity,  $k_{eq}$ , from the heat equation  $\vec{q}'' = -k \vec{\nabla} T$  [7], [8]. A review of the traditional analytic models to obtain  $k_{eq}$  is detailed in [9]. Some of these methods are used in [10] to get the effective conductivity of bundles of litz wire for electrical machines.

In this paper, one step further is carried out and the homogenization is applied at two levels. The first one, described in Section II-A, includes the conductor and its insulation. The latter is applied at winding level, where the wires and the material between them (air or potting resin) are homogenized, explained in Section II-B. An application example is depicted in Fig. 1.

The main features of the proposed method are:

- Simplified thermal analysis of the winding while keeping a good accuracy, since the equations are based on FEA results.
- Reduction of the running time of 3D thermal simulations by a factor between 6 and 8, compared with detailed simulations, due to the resulting simpler mesh.
- Assured convergence of 3D thermal simulations, which

allows the analysis of complex problems.

This two-level homogenization for magnetic components was introduced in [11]. A simplification of the set of equations and some explanations to extend this approach to model inductors and transformers with any winding type are presented in this paper.

The paper is structured as follows: in Section II the concept is described. It involves a two-step homogenization. The first step is at wire level, explained in Subsection II-A for round solid wires and litz bundles, with round or square section. Afterwards, the second step is applied at winding level, for round solid or litz, square litz and foil winding. It is described in Subsection II-B. Then, the application of the two-level homogenization for transformers is particularized in Section III, in which some especial concern needs to be considered if interleaving technique or insulation between layers are used. In Section IV the method is experimentally validated with DC and AC excitation and the reduction of the simulation time for 3D FEA is analyzed. Finally, conclusions are presented in Section V.

## II. THE METHOD: TWO-LEVEL HOMOGENIZATION

The proposed two-stage homogenization is described in this Section. The first step, described in Section II-A, comprehends the conductor and its insulation. The latter, explained in Section II-B, is applied at winding level, where the wires and the material between them (air or potting resin) are homogenized. Fig. 2 shows a diagram of the method.

### A. Wire level homogenization

The first step is to homogenize the conductor and insulation materials. The process to homogenize different conductor types (round solid wire, round and square litz) for any magnetic component is discussed along the next subsections.

1) **Round solid wire:** In this case, there is no homogenization strictly speaking. Nevertheless, a simplification is required in order to avoid an excessively restrictive mesh of the wires: its insulation should be neglected. This simplification does not compromise the temperature estimation since the temperature gradient within a conductor and in the insulator is negligible. The reasons for this are the reduced dimensions of the wire, the high thermal conductivity of the conductor and its internal heat generation. This assumption is valid for commercial wires lower than AWG 10 (external diameter of 2.59 mm) [7], used for low and medium power applications (< 100 kW).

Additionally, since the insulator thickness of common commercial solid wires is below the *critical radius* value ( $r_{crit} = k_i/h = 0.04\text{W/m}\cdot\text{K} / 5\text{W/m}^2\cdot\text{K} = 8\text{ mm}$  for common operating conditions) [7], [8], it is reasonable to consider that the effective thermal conductivity of the whole wire is equal to the conductor material conductivity ( $k_w = k_{cond}$ ). More details regarding the *critical radius* can be found in [7] and [8].

Furthermore, the thermal conductivity has a dependence on temperature. However, the conductivity of copper and aluminium wires can be assumed constant and equal to 401W/m·K and 237W/m·K respectively, for a temperature range between 0°C and 100°C [12].

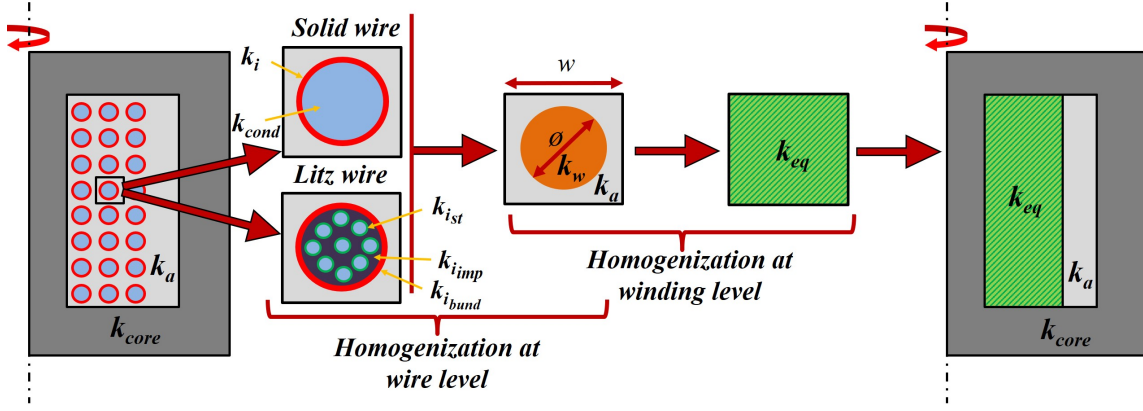


Fig. 2. Design flow to model the winding thermal equivalent layer (pot core is used as an illustrative example). From left to right: cross-sectional area of a pot core inductor, as an example; homogenization at wire level and at winding level; inductor with the equivalent layer.

2) **Litz wire with round or square section:** This is another usual case. Due to the high number of strands within a litz bundle and their reduced diameter, the homogenization of the bundle is required to make possible its thermal analysis. Different methods are discussed next.

It is important to distinguish between two different types of litz wire: impregnated (the strands from a bundle are embedded within a potting material) and non-impregnated (no potting is used in the bundle). A study in [13] reveals that Hashin-Shtrikman's method for two-phase composite materials [14] is more suitable for impregnated ones – a comparison with experimental results is provided in that paper to validate this statement– for which the thermal properties of the impregnation and insulation materials are close and might be considered equal. Then, the conductivity of the bundle,  $k_w$ , can be described as:

$$k_w = k_i \cdot \frac{(1 + \tau) \cdot k_{cond} + (1 - \tau) \cdot k_i}{(1 - \tau) \cdot k_{cond} + (1 + \tau) \cdot k_i} \quad (1)$$

Where  $k_{cond}$  is the conductor strand conductivity,  $k_i$  is the insulator conductivity and  $\tau$  is the volume fraction of conductor material ( $\tau = vol_{cond}/vol_{tot}$ ). However, the error due to the previous assumption might be unacceptable if the impregnation and insulation materials's properties cannot be assumed as equal. In [15], the use of  $k'_i$  instead of  $k_i$  in (1) to account for the different conductivity of the insulator ( $i_{st}$  subscript) and impregnation ( $i_{imp}$ ) materials. The definition of  $k'_i$  is:

$$k'_i = \frac{k_{i_{st}} \cdot v_{i_{st}} + k_{i_{imp}} \cdot v_{i_{imp}} + k_{i_{bund}} \cdot v_{i_{bund}}}{v_{i_{st}} + v_{i_{imp}} + v_{i_{bund}}} \quad (2)$$

The corresponding volume fraction of each material ( $v$  and the corresponding subscripts) can be calculated with the Packing Factor ( $PF$ ), usually provided by the manufacturer. Furthermore, an additional term is added to consider the conductivity of the external cover insulator of the bundle, designated by the subscript *bund*. This modification of the Hashin-Shtrikman's approach shows an error in the estimation

of  $k_w$  compared with measurements lower than 11 % for low packing factor litz bundles ( $PF < 50\%$ ) and lower than 37 % for high packing factor bundles ( $PF > 50\%$ ), according to [15].

For higher packing factor ( $PF > 50\%$ ), other methods have been recently presented. In [16], a thermo-electric field analogy to estimate the effective  $k_w$  of litz bundles is developed. A deviation from measurements between 1.3 % and 12.5 % is achieved with this approach, but it is a relatively complex method. The methodology from [17] and [18] is based in thermal networks. Both use the available data from the manufacturer and provide good matching with FEA results. The first one provides different models for square-packed and hexagonal-packed wires, but does not offer experimental data. The second one provides experimental results with good accuracy. However, it requires some experimental calibration, since there is a strong dependence on the uncertainty associated to manufacturing tolerances and material data provided by the litz manufacturers. By analyzing the results from [18], it can be stated that this error margin is lower than 34 %. Therefore, using the modified Hashin-Shtrikman's method from [15] leads to results close or within that uncertainty band.

To summarize, Hashin-Shtrikman's method with the averaged properties of the insulation materials offers proper accuracy for low packing factor values. For higher values, other methods like the ones provided in [17] and [18] are recommended, but require additional complexity or calibration with measurements due to the manufacturing uncertainty. In that case, modified Hashin-Shtrikman's method (1) and (2) can be used for simplicity, since its accuracy is acceptable. As described in Section IV, this approach offers a good matching with experimental results.

## B. Winding level homogenization

Once the homogeneous conductivity of a wire,  $k_w$ , is obtained the next step is to characterize the effective thermal conductivity of the whole winding of the magnetic component,  $k_{eq}$ . This comprises every homogenized wire ( $k_w$ ) and the surrounding material between them (Fig. 2).

This second homogenization implies the geometric transformation of every homogenized wire to a single block. As

a result, the external heat exchange surface with the air is slightly modified, as well as the contact resistance between the equivalent winding and the core. However, this effect has been neglected, since its contribution have a minimum effect on the global heat transfer.

It is important to highlight that uniform power distribution is assumed. The power losses generated in the original system remain unchanged in the equivalent model. As an example, to analyze an inductor with 100 wires and 2 W total winding losses, the 2 W will be assigned to the equivalent block.

The guidelines to model round wires (solid and litz), square litz wire and foil for inductors are described along the next subsections.

1) **Round wires (solid and litz):** The analytical homogenization techniques summarized in [10] could be use to calculate  $k_{eq}$  for round wires (solid or litz). However, their accuracy is limited for low filling ratios, which is common in composite materials for which they were developed. On the other hand, the wires in a magnetic component usually arranged very close to each other, leading to high filling ratios within the window. Then, those approaches are not recommended and a more accurate model is required.

A new generalized model based on a multivariable curve fitting of FEA simulation results is introduced in this paper in order to increase the accuracy and avoid the previous limitation. The simulation setup is depicted in Fig. 3, similar to the process to obtain the effective thermal conductivity described in [7] and [8]. The depicted 'cell' is a representative cross-section sample of the winding, as shown in Fig. 2. This cell contains a wire (with conductivity  $k_w$ ) and the surrounding material (i.e. potting resin or air, with conductivity  $k_a$ ). The diameter of the wire is  $\phi$  and the width of the representative cell is  $w$ . Since this cell is 'repeated' along the window of the magnetic component, the top and bottom surfaces are defined as adiabatic, to account for this symmetry [7]. Then, since the goal of this analysis is to obtain the effective thermal conductivity across the cell, certain heat flux,  $q_x''$  [W/m<sup>2</sup>], is injected on the left surface of the cell. As a consequence, a temperature gradient appears between the left and the right surfaces, considering  $T_1$  and  $T_2$  as the average surface temperatures in [K] on left and right surfaces respectively. Hence, the effective thermal conductivity,  $k_{eq}$ , between left and right surfaces is calculated as the product of the applied heat flux ( $q_x''$ ) and the width of the cell ( $w$ ) divided by the temperature rise between surfaces ( $\Delta T = T_1 - T_2$ ), according to (3).

$$k_{eq} = q_x'' \cdot \frac{w}{\Delta T} = q_x'' \cdot \frac{w}{T_1 - T_2} \quad (3)$$

The effective thermal conductivity of the winding,  $k_{eq}$ , depends on the ratio between the thermal conductivity of the wire and the surrounding material,  $k_{ratio} = k_w/k_a$ , and their volume fractions, which can be expressed in terms of the relationship between the diameter of the wire over the width of the cell,  $\phi/w$ . Obtaining this relationship by analytical methods becomes quite complex, therefore 2D FEA simulations are used instead (according to the setup shown

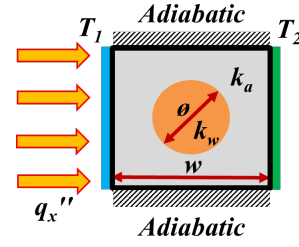


Fig. 3. Cross-sectional representation of the simulation setup.

in Fig. 3). In order to get the effective conductivity for any combination of size and conductivity ratios, a high enough number of simulations are solved. In this case, a sweep of 31 steps from 0.5 and 0.8, and 100 more from 0.8 to 0.998 for  $\phi/w$  are considered. On the other hand,  $k_{ratio}$  is swept with 600 logarithmic steps from  $10^0$  to  $10^5$ . For each combination of  $k_{ratio}$  and  $\phi/w$ , the effective thermal conductivity,  $k_{eq}$ , is obtained by simulation. These results are shown in Fig. 4.

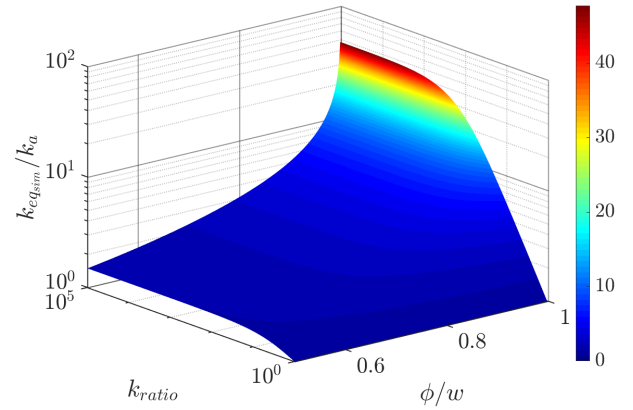


Fig. 4. Effective thermal conductivity of a cell: simulation results of  $k_{eq}/k_a$  over  $k_{ratio}$  and  $\phi/w$ .

Then, a multivariable fitting of the resultant graph was performed to get a general expression for  $k_{eq}$ , applicable to any  $k_{ratio}$  from 1 to 100000 and  $\phi/w$  from 0.5 to 1 —for lower size ratios, any of the traditional methods can be used, since they offer a negligible error. To do so, (4) is proposed. It consists of a modification of Hashin-Shtrikman's equation, where the volume fraction  $\tau$  is replaced by a variable  $\tau^*$ , described next.

$$\frac{k_{eq}}{k_a} = \frac{(1 + \tau^*) \cdot k_{ratio} + (1 - \tau^*)}{(1 - \tau^*) \cdot k_{ratio} + (1 + \tau^*)} \quad (4)$$

Where  $\tau^*$  is a variable obtained such that its value makes (4) to get the exact value of  $k_{eq}$  from the simulations. It is expressed as:

$$\tau^* = \frac{\pi}{4} \cdot \left(\frac{\phi}{w}\right)^2 + a \cdot \left(\frac{\phi}{w}\right)^b + c \cdot \left(\frac{\phi}{w}\right)^d \quad (5)$$

Whose coefficients  $a$ ,  $b$ ,  $c$  and  $d$  are expressed in terms of  $k_{ratio}$  according to Equations 6. Notice that coefficients  $c$  and  $d$  are 0 for  $k_{ratio}$  lower than 6.7; their values depend on  $k_{ratio}$ :

$$a = \frac{0.15323 \cdot k_{ratio} - 0.21445}{k_{ratio} + 6.1801} \quad (6a)$$

$$b = \frac{14.297 \cdot k_{ratio} + 78.569}{k_{ratio} + 8.3734} \quad (6b)$$

$$c = \begin{cases} 0 & k_{ratio} < 6.7 \\ \frac{0.04902 \cdot k_{ratio} - 0.24267}{k_{ratio} + 19.568} & 6.7 \leq k_{ratio} \end{cases} \quad (6c)$$

$$d = \begin{cases} 0 & k_{ratio} < 6.7 \\ \frac{270.55 \cdot k_{ratio} - 472.41}{k_{ratio} + 3.6959} & 6.7 \leq k_{ratio} \end{cases} \quad (6d)$$

The results obtained by (4) are compared to the aforementioned approaches from [10] (Hashin-Shtrikman, Maxwell, Rayleigh and Milton) and FEA results. To make this comparison, the relative error ( $Error[\%] = (k_{estimated}/k_{simulated} - 1) \cdot 100$ ) for those approaches is plotted over  $\phi/w$  and  $k_{ratio}$  in Fig. 5. It can be seen that Hashin-Shtrikman, Maxwell and Rayleigh methods might result in an underestimation of  $k_{eq}$  of 83%, 95% and 88%, respectively. The mismatch of Milton's approach varies from +18% to -75%. This could lead to unacceptable estimations of the temperature rise. However, the proposed method shows a better performance, with a little error in the band of  $[-2.4, 4.6]\%$ . This fact reveals that the developed method shown in this paper is more suitable for the homogenization of round conductors than other traditional approaches.

2) **Square litz wires:** Since square litz wires lead to high filling factor of the magnetic component's window, the space between the bundles is negligible. Then, only the first step of the homogenization is required. The procedure to obtain an equivalent thermal conductivity in this case correspond to the

described in Section II-A2. The equivalent conductivity of the winding will be equal to the obtained  $k_w$  in that section.

3) **Foil:** Foil is a useful choice for high frequency specifications [19] and provides a lower thermal impedance path than litz or solid wires, since the heat exchange surface between layers is much higher. The homogenized thermal conductivity of a foil winding can be easily obtained if there is no insulation. In that case, the equivalent conductivity of the winding can be approximated to the conductor's conductivity, neglecting the air between the layers. However, if some insulation layer exists between the conductor layers, the effective thermal conductivity requires some further calculations, depending on the shape of the winding (rectangular or circular). To analyze these problems, 1D heat transfer equation can be solved to get effective thermal conductivity of the winding for each spatial direction, as described next:

#### • XY rectangular winding:

If the center core leg is squared and the conductor and the insulation layers are alternated, a simple thermal network in cartesian coordinates can be analyzed to extract the effective conductivity for each spatial direction: *a*) orthogonal direction ( $k_{eq_{ort}}$ ) across the perpendicular direction to the winding; *b*) top-down direction ( $k_{eq_z}$ ) along the vertical direction of the winding; *c*) tangential direction ( $k_{eq_{tan}}$ ) along the winding direction.

Solving the corresponding one-dimensional thermal networks corresponding to Fig. 6 (see Appendix A for further details), the thermal conductivity in the orthogonal directions is defined as:

$$\frac{1}{k_{eq_{ort}}} = \frac{1}{k_{cond}} \cdot \frac{l_{cond}}{l_{cond} + l_{ins}} + \frac{1}{k_{ins}} \cdot \frac{l_{ins}}{l_{cond} + l_{ins}} \quad (7)$$

Where  $l_{cond}$  and  $l_{ins}$  are the total width of conductor and insulation layers, respectively. As an example, in Fig. 6, considering the red layers as conductors and yellow ones as

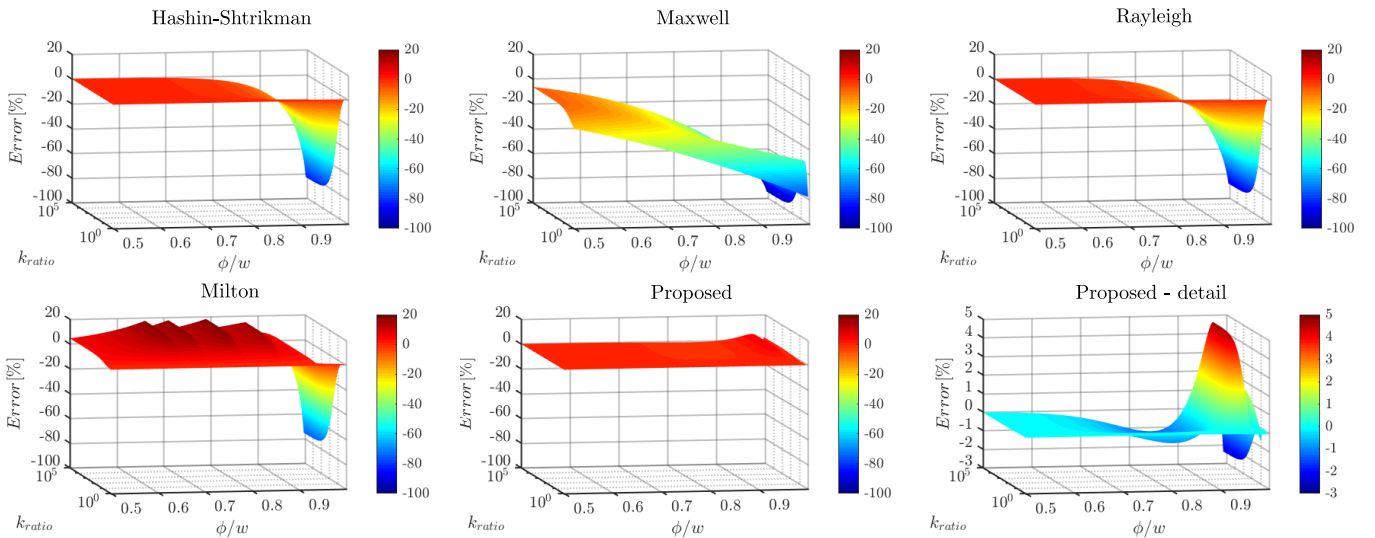


Fig. 5. Relative error in the estimation of the effective thermal conductivity calculated with traditional approaches and the proposed method.

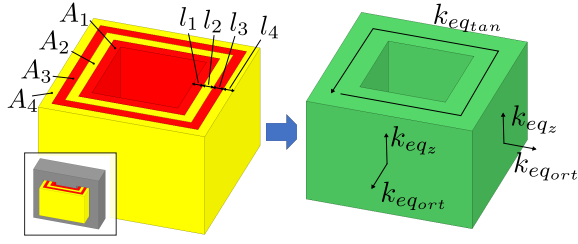


Fig. 6. Foil winding for squared cores (left) and equivalent winding (right).

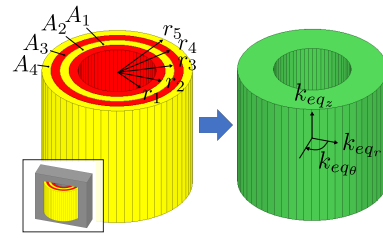


Fig. 7. Foil winding for round cores (left) and equivalent winding (right).

insulation,  $l_{cond} = l_1 + l_3$  and  $l_{ins} = l_2 + l_4$ );  $k_{cond}$  and  $k_{ins}$  are their corresponding conductivity.

Regarding the vertical direction, the conductivity can be expressed as:

$$k_{eqz} = k_{cond} \cdot \frac{A_{cond}}{A_{cond} + A_{ins}} + k_{ins} \cdot \frac{A_{ins}}{A_{cond} + A_{ins}} \quad (8)$$

Where  $A_{cond}$  and  $A_{ins}$  are total heat exchange cross sections of both the conductor and the insulation tape ( $A_{cond} = A_1 + A_3$  and  $A_{ins} = A_2 + A_4$ ).

Finally, the impact of the tangential conductivity on the heat flow along this direction can be ignored, since the temperature gradient along the same foil layer is negligible because the winding is a heat source itself and it has axial symmetry. Thus, the problem is similar to a composite plane wall.

#### • RZ Circular winding:

In a similar manner, a one-dimensional thermal network is analyzed in cylindrical coordinates to get an equivalent conductivity when a round center core leg is studied. This case is shown in Fig. 7 (see Appendix A for further details). The radial component of the equivalent conductivity is expressed as:

$$k_{eqr} = \frac{\ln\left(\frac{r_n}{r_1}\right) \cdot k_{cond} \cdot k_{ins}}{k_{ins} \sum_{n_{cond}} \ln\left(\frac{r_{n+1}}{r_n}\right) + k_{cond} \sum_{n_{ins}} \ln\left(\frac{r_{n+1}}{r_n}\right)} \quad (9)$$

Where  $n_{cond}$  refers to the conductor layers and  $n_{ins}$  to the insulation layers (in the example in Fig. 7:  $n_{cond} = 1, 3$  and  $n_{ins} = 2, 4$ ).

The conductivity along the vertical direction is described in (8). Finally, the impact of the conductivity along the  $\theta$

direction can be ignored, due to the same reasoning than  $k_{eqtan}$  previously described.

#### C. Summary

Finally, the two-level homogenization process is summarized in Table I for the different winding types, to ease the readability. In any case, additional design steps from Section III will be followed if interleaving or insulation are used.

### III. USE OF THE TWO-LEVEL HOMOGENIZATION FOR TRANSFORMERS

So far, the procedure to homogenize a magnetic component made by a single winding type has been explained. That is the typical case of an inductor. However, if different wires (size or type) are used in the same component, some further steps need to be carried out. A clear example of this is a transformer, in which the diameter of the wires from primary and secondary is different.

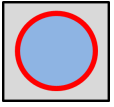
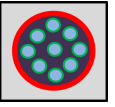
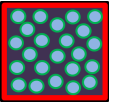
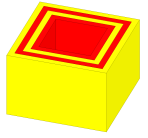
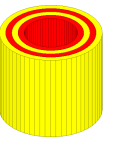
Some considerations to apply the introduced method to transformers, where interleaving techniques and insulation tape might be used, are described in this section.

#### A. Application to different interleaving levels

The different levels of interleaving are depicted in Fig. 8 and described next:

- Winding arrangement in blocks. Primary and secondary windings are separately treated since the diameter of their wires could be different, as well as their losses. Then, the corresponding effective thermal conductivity for each winding,  $k_{eq1}$  and  $k_{eq2}$ , is calculated according to Section II.

TABLE I  
EQUATIONS SUMMARY FOR DIFFERENT WINDING TYPES

				
<b>Round solid wire</b>	<b>Round litz bundle</b>	<b>Square litz bundle</b>	<b>Square foil</b>	<b>Round foil</b>
1) $k_w = k_{cond}$ .	1) $k_w$ (Eq. 1 and 2).	1) $k_{eq} = k_w$ (Eq. 1 and 2).	1) $k_{eqort}$ (Eq. 7).	1) $k_{eqr}$ (Eq. 9).
2) $k_{eq}$ (Eq. 4-6).	2) $k_{eq}$ (Eq. 4-6).		2) $k_{eqz}$ (Eq. 8).	2) $k_{eqz}$ (Eq. 8).

- (b) Layer level interleaving. The procedure to compute  $k_{eq1}$  and  $k_{eq2}$  do not differ from the previous case but the corresponding equivalent blocks are alternated according to the primary and secondary arrangement.
- (c) Fully interleaved winding. Since primary and secondary wires are alternated within the same layer, the only solution is to homogenize the whole winding as one single block. First, the effective thermal conductivity of each cell is calculated ( $k_{eq1}$  and  $k_{eq2}$ ). Then, (8) is used to obtain the effective conductivity of each layer. Finally, depending on the shape of the center leg of the magnetic component, the corresponding equations from Section II-B3 will be used to get the total effective conductivity,  $k_{eqTOT}$ .

- **Losses assignation**

It is important to notice that an electromagnetic (EM) homogenization is required prior to perform the thermal simulation to consider the non-uniform losses distribution due to high-frequency effects. Some EM homogenization techniques are proposed in [20]–[23]. By using these approaches, both the EM and thermal simulations can be coupled in the simulation software. Further details are provided in Section IV-B.

In the case that the EM-thermal coupling was not an available feature of the used simulation tool, certain simplifications could be performed depending on the interleaving level. For a winding arrangement in blocks, (a), the total primary losses  $P_{pri}$  and total secondary losses  $P_{sec}$  would be assigned to the blocks  $k_{eq1}$  and  $k_{eq2}$ , respectively (see Fig. 8). For a layer level interleaving, the assigned losses to each equivalent layer would correspond to the proportional part of the number of layers

( $N_{layers_1}$  and  $N_{layers_2}$ ). For example, if primary winding dissipates 1 W and there are 5 layers, the losses will be equally split among them ( $1 \text{ W}/5 = 0.2 \text{ W}$  per primary layer). Finally, in a fully interleaved winding, since both primary and secondary windings are homogenized as a single block, the assigned losses to this block would be equal to the total winding losses. However, using these simplifications would penalize the accuracy of the obtained temperature compared to the EM-thermal coupling. Then, it is recommended to use EM-thermal coupling if possible.

### B. Insulation tape between layers

It is a common practice to add some insulation tape, usually between primary and secondary winding in a transformer. As an example, the process to model this cases is depicted in Fig. 9. The first step (from 1) to 2)) is to homogenize each conductor, according to Section II-A (wire level homogenization), obtaining their  $k_w$ . Next, each layer separated between tape layers is homogenized, following the procedure from Section II-B (winding level homogenization), assigning to them their corresponding  $k_{eq}$  (step 3)). Optionally, every insulation tape and winding layer can be homogenized in a single block with conductivity  $k_{eqTOT}$ , by treating them as foil layers, using the corresponding equations from Subsection II-B3 (step 4)).

At this point, the procedure to obtain a simplified thermal model for any inductor or transformer with round, square or foil winding, also with interleaving or insulation if needed, is explained. The method is validated by means of experimental results in the next Section.

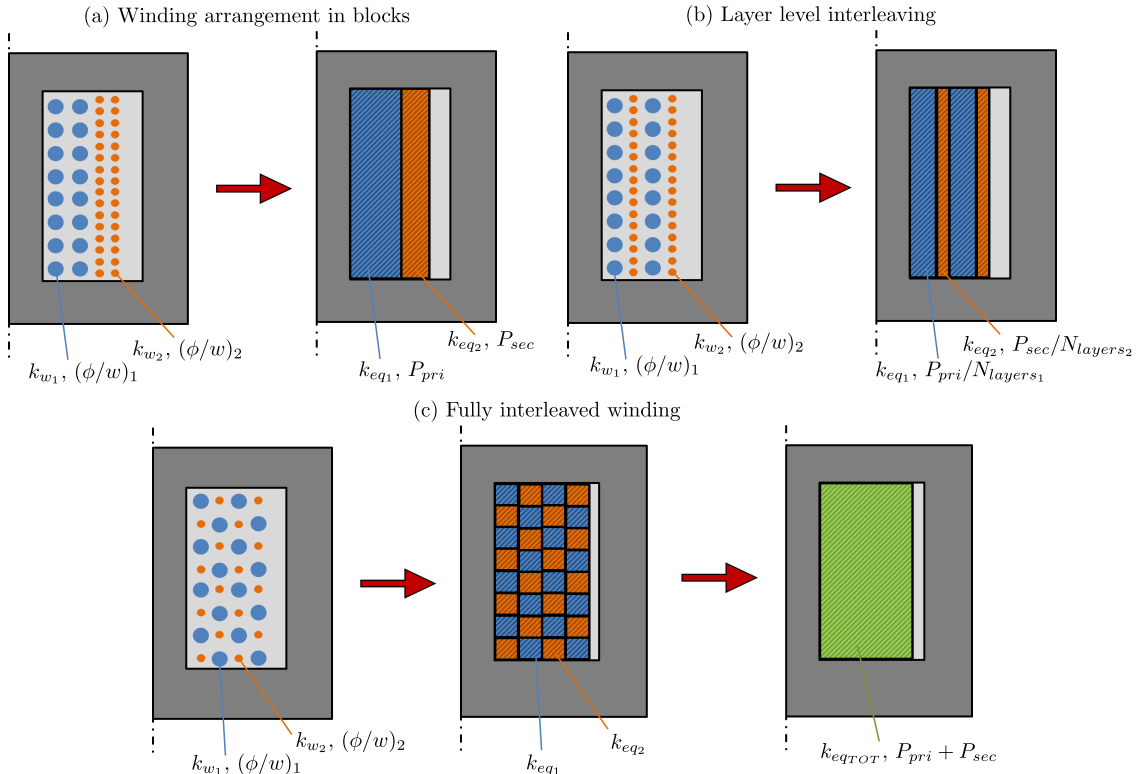


Fig. 8. Homogenization procedure for different winding arrangements in transformers.

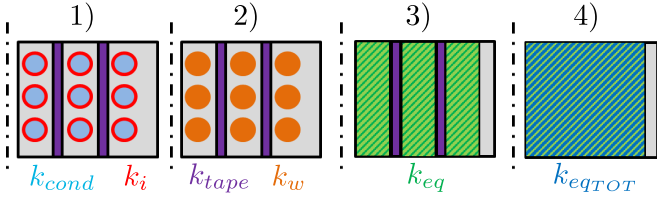


Fig. 9. Representation of a winding modeling with insulation tape: 1) Original winding; 2) First homogenization; 3) Second homogenization; 4) Tape and winding layers homogenization.

#### IV. EXPERIMENTAL VALIDATION OF THE MODEL

In this section, the scope of the suggested homogenization technique is analyzed and validated in two different scenarios: DC and AC excitation currents. The corresponding testbench is depicted in Fig. 10. In (a), the device under test (DUT) is connected to a voltage source at constant voltage, so a DC current is injected to the magnetic component. In (b), a sinusoid is provided by a waveform generator (GW Instek, model AFG-2005), which is amplified by an RF amplifier (AR, model 150A 100B) and then connected to the magnetic component in order to analyze the high-frequency effects of an AC current. In the case of an inductor, (b.1), it is connected in series to a capacitor. The impedance of this resonant series LC tank is minimum at its resonant frequency, with the purpose of injecting a high peak current with an acceptable voltage level at that frequency. In the case of a transformer, (b.2), a resistive load of  $1\Omega$  is connected in its secondary side in order to have AC current flowing through both primary and secondary windings.

As a result of injecting either DC or AC current, some electromagnetic losses are caused in the tested magnetic component. Then, its temperature starts rising until the thermal steady-state is reached. The goal of this testbench is obtaining experimental measurements of this temperature rise and com-

pare it with a detailed 3D FEA simulation ('wire level FEA') and other 3D FEA simulation using the method developed in this paper ('winding level FEA'). The differences between both simulations are described next:

- 'Wire level FEA'. Fully detailed 3D FEA simulations which include the insulation of the wires or the strands within a litz bundle are not feasible due to the highly demanding meshing of these objects [21]. As a result, at least the wire level homogenization described in Section II-A is mandatory and applied in these 'Wire level FEA' 3D simulations.
- 'Winding level FEA'. In this case, the suggested two-step homogenization is used, every wire from the previous step and the material between them are homogenized, according to Sections II-B and III. This two-step homogenization leads to a considerably reduced simulation time compared with the 'Wire level FEA' approach, which will be analyzed at the end of this section.

To compare both 3D simulations with the experimental results, mean surface temperatures of the core and the winding of each magnetic component are measured with a FLUKE-Ti400 thermal camera, according to the procedure described in [24]–[26]. The 3D simulations are performed with Icepak, from ANSYS Electronics Desktop 2019.1.

Several inductors and a transformer, with different core shapes and winding types, are tested to validate the introduced homogenization method under different scenarios, described in Table II. The next thermal conductivity has been considered for the different objects or materials in all cases:  $k_{fe} = 4.5$  [W/m·K] for the ferrite cores [27],  $k_a = k_{imp} = 0.03$  [W/m·K] (conductivity of air at 353 [K] from [28]) for the air surrounding the wires and the 'impregnation material' of the litz bundles,  $k_{i_{bund}} = 0.155$  [W/m·K] and  $k_{i_{st}} = 0.245$  [W/m·K] [16] for the bundle insulation and strand insulation materials. The accuracy and simulation speed results are analyzed along the next subsections.

The results presented for each prototype are calculated in 3D simulations and extracted from the thermography (FLUKE Smart View software). The measurements from the thermal camera are considered as the reference for the surface temperatures. Then, the relative error between the measured temperature rise ( $\Delta T_{exp} = T_{exp} - T_{amb}$ ) and the temperature rise obtained by the corresponding 3D simulation ( $\Delta T_{sim} = T_{sim} - T_{amb}$ ) is calculated according to (10).

$$Error_{T_{surf}}[\%] = \left( \frac{\Delta T_{sim}}{\Delta T_{exp}} - 1 \right) \cdot 100 \quad (10)$$

Regarding the maximum temperature estimation, since measuring the temperature within the core is not possible, only the results from 'Wire level FEA' (just wires/bundles are homogenized) and 'Winding level FEA' (two-stage homogenization is performed) 3D simulations are compared. In this comparison, the 'Wire level FEA' is considered as the reference, so the relative error of these magnitudes is calculated with (11).

$$Error_{T_{max}}[\%] = \left( \frac{\Delta T_{windFEA}}{\Delta T_{wireFEA}} - 1 \right) \cdot 100 \quad (11)$$

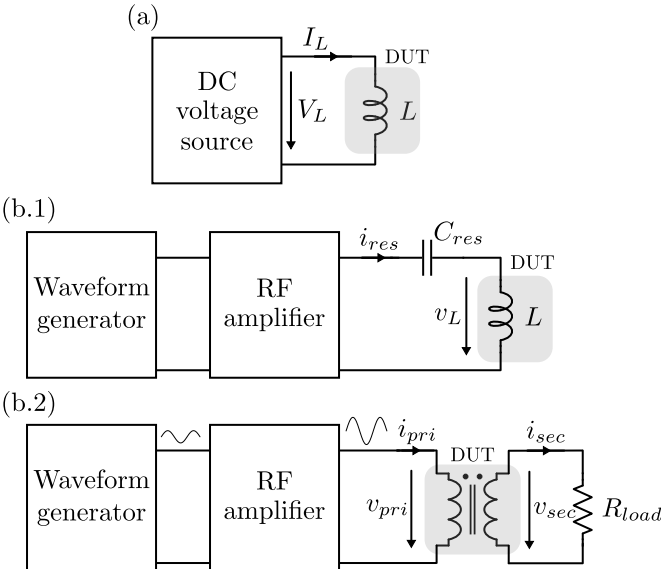


Fig. 10. Testbench for (a) DC excitation in inductors, and AC excitation in (b.1) inductors and (b.2) transformers.

TABLE II  
DESCRIPTION OF THE TESTED PROTOTYPES

Prototype	A (inductor)	B (inductor)	C (inductor)	D (inductor)	E (transformer)
Core	P36/22	P36/22	PQ32/30	PQ32/30	RM8/I
Winding type	Solid	Litz 35 x 0.2mm	Litz 35 x 0.2mm	Foil (0.27mm·2) (cop.+iso.+cop.+iso.)	Solid
$\phi$ [mm]	0.81 (AWG20)	1.45 (AWG15)	1.45 (AWG15)	—	pri=0.51 (AWG24), sec=0.81 (AWG20)
insulation thickness[mm]	0.02	0.055	0.055	65 $\mu$ m (·2)	0.02
$w$ [mm]	0.87	1.6	1.6	4	pri=0.64, sec=1
Number of turns	92	28	42	22	pri=28, sec=15
$k_w$ [W/m·K]	390	0.205309	0.205309	390	390
$k_{eq}$ [W/m·K]	0.179535	0.079864	0.079864	1.4094	pri=0.0639, sec=0.0721

### A. DC tests

In this section, some DC current is injected into the inductors 'A', 'B', 'C', 'D' in order to have certain winding conduction losses while having null core loss, according to the setup depicted in Fig. 10. Power loss and ambient temperature for each test are summarized in Table III. The temperature distribution obtained with the thermal camera and the suggested 3D 'Winding level FEA' simulations corresponding to this tests is shown in Fig. 11. Mean and maximum temperatures in the core and the winding of each device are analyzed next to validate the proposed model for DC excitation.

TABLE III  
DC TEST CONDITIONS

Prototype	A	B	C	D
$T_{amb}$ [°C]	26	24	26	20
$P$ [W]	3.793	3.244	3.160	4

For each prototype, the results are presented in bar graphs. The bars respectively correspond to the experimental, 'Wire level FEA' and 'Winding level FEA' obtained temperatures (bars for experimental maximum temperatures are not shown since that data is not available). The error margin inherent to the measurements, which is related to the discrepancy of the measured surface emissivity and the background radiation, is included for every case.

#### 1) Prototype A: Inductor, P36/22, round solid copper:

As a proof of concept of the homogenization at winding level (Section II-B), a pot core inductor with round solid wire is built. Since the winding is practically surrounded by the core, the external boundary conditions practically do not affect it, thus avoiding a possible source of error. The results of this test are shown in Fig. 12. It can be seen that the simulation with the equivalent layer ('Winding level FEA') deviates only a 5 % for the winding surface temperature estimation ( $T_{w_{surf}}$ ) and  $-2.2$  % for the core surface temperature ( $T_{c_{surf}}$ ). Furthermore, the evaluation of the maximum temperatures in

winding ( $T_{w_{max}}$ ) and core ( $T_{c_{max}}$ ) respectively have  $-7.5$  % and  $-4.4$  % deviation, compared with the detailed 'Wire level FEA' simulation.

2) **Prototype B: inductor, P36/22, round litz:** Prototype B consists in an inductor, with the same core than the previous one, but with round litz wire. In this case, the performance of both wire-level (SectionII-A) together with the winding-level homogenization (SectionII-B) can be checked. The data of the litz wire provided by the manufacturers has certain tolerance, so there is some uncertainty. However, the results of the 'Winding level FEA' simulation are close to the 'Wire level FEA' estimations, as depicted in Fig. 13. The evaluation of  $T_{w_{surf}}$  has almost no deviation compared with the experimental measurement (1 % and  $-3.7$  % respectively) and a slightly higher for  $T_{c_{surf}}$  (9.2 % and 10.1 %). This might be due to a mismatch of the boundary conditions in the simulations with respect to the experimental setup.

Comparing prototypes 'A' and 'B', they use both a P36/22 core, but 'A' is made by solid wires and 'B' by litz bundles. After the 'winding homogenization', the wires are replaced by a block. This change in the geometry leads to a different external surface exposed to the ambient (lower external surface after the homogenization). Since the solid wires from 'A' are more compactly packed than 'B', the decrement of external surface is lower in 'A' than in 'B'. Consequently, the impact of convective heat transfer is stronger in 'A' than in 'B' after the winding homogenization. This is the reason why the maximum winding temperature after the homogenization is higher after the winding homogenization (two-level homogenization) in 'A' and lower in 'B', compared with their corresponding wire homogenization (first level homogenization).

However, the important point here is that the 'Winding level FEA' simulation offers close results to the 'Wire level FEA', but with a much less demanding mesh and thus a lower simulation time, which will be analyzed at the end of this section.

3) **Prototype C: inductor, PQ32/20, round litz:** Once the performance of the two-step homogenization is checked, a PQ core inductor is built to check the performance of the

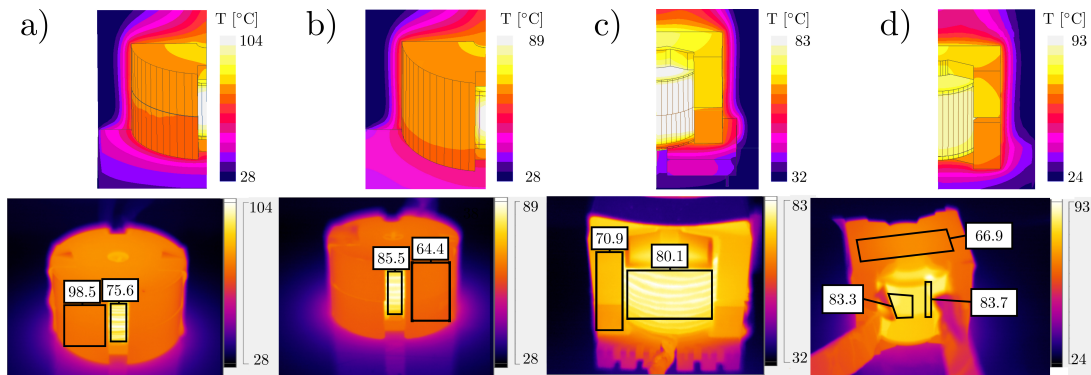


Fig. 11. DC test thermal results: on the upper row, results of the 'Winding level FEA' 3D thermal simulations of the prototypes A, B, C and D from left to right; on the bottom row, the corresponding experimental thermography including the averaged temperature in the marked black squares.

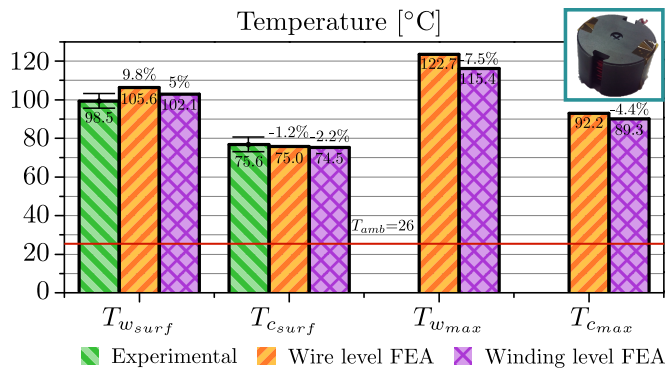


Fig. 12. DC test temperature of 'A' (P36/22 inductor, round solid wire).

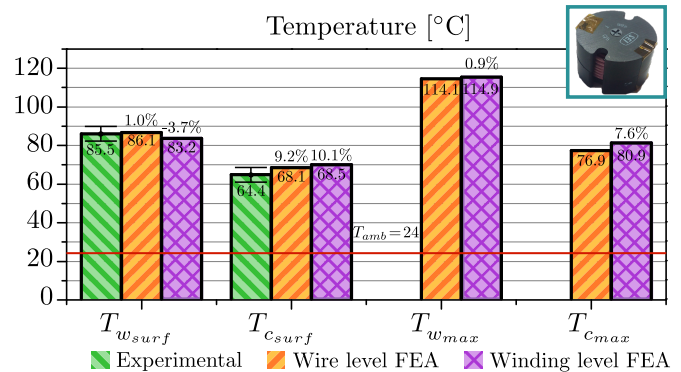


Fig. 13. DC test temperature of 'B' (P36/22 inductor, round litz bundle).

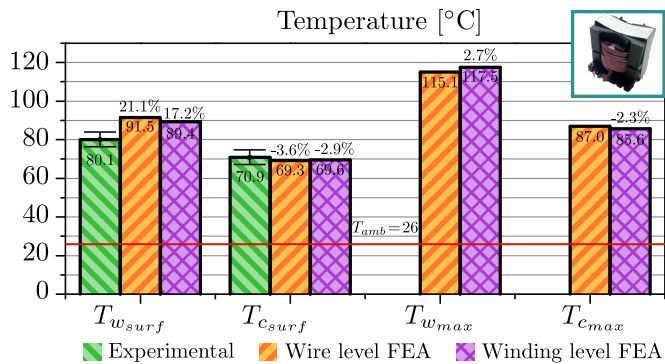


Fig. 14. DC test temperature of 'C' (PQ32/20 inductor, round litz bundle).

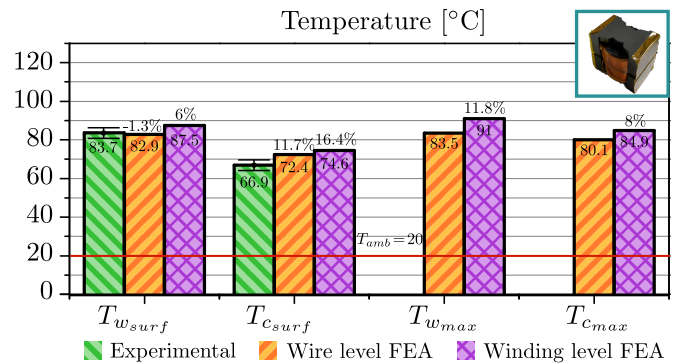


Fig. 15. DC test temperature of 'D' (PQ32/20 inductor, foil).

equivalent layer when it is in direct contact with the ambient. Due to the addition of this condition, another uncertainty appears, as previously explained. This is the reason of a higher deviation of  $T_{w_{surf}}$  (Fig. 14). But still, the highlight of this comparison is the similarity of the results of both simulations, so the 'Winding level FEA' simulation offer the additional advantage of having a much simpler mesh.

4) **Prototype D: inductor, PQ32/20, foil:** Another concept presented in this paper is the homogenization of foil wound magnetic components. To validate the expressions from Section II-B3, a PQ core inductor with foil winding is built. As shown in Fig. 15, the estimation of  $T_{w_{surf}}$  and  $T_{c_{surf}}$  has an acceptable deviation from the measurements. Comparing this case with the previous ones, the evaluation of the maximum

temperatures are slightly higher with the 'Winding level FEA' model.

## B. AC tests

Along this section, AC excitation is used instead of DC in every inductor (prototypes 'A', 'B', 'C' and 'D'). A transformer is added (prototype 'E'), where proximity effect becomes more critical. In AC excitation, some local effects within the wires appear (skin and proximity effects), but the resultant loss distribution can be directly mapped in the thermal simulation [29]. The AC setup is depicted in Fig. 10. The peak-to-peak of the sinusoidal current and frequency for each case (equal to the resonant frequency of the LC tank), as well as the ambient temperature, are summarized in

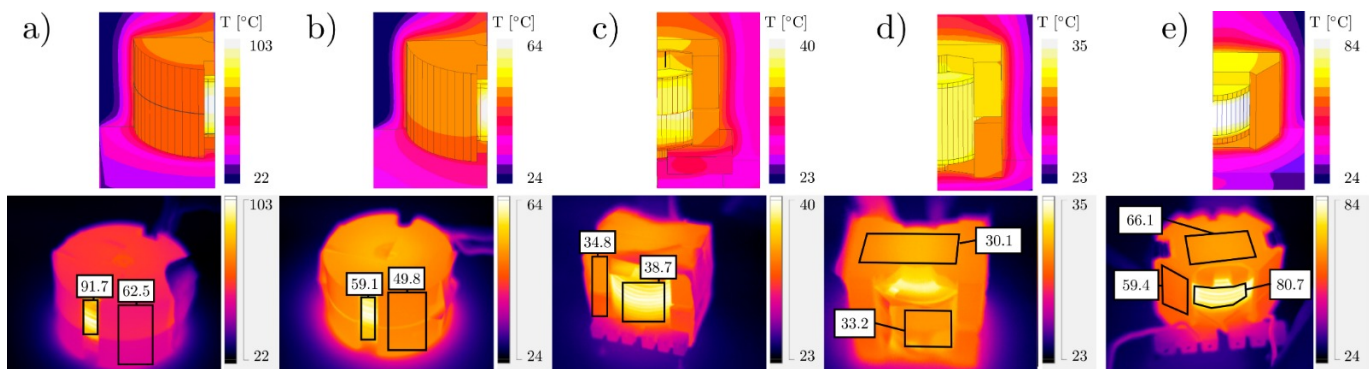


Fig. 16. AC test thermal results: on the upper row, results of the 'Winding level FEA' 3D thermal simulations of the prototypes A, B, C, D and E from left to right; on the bottom row, the corresponding experimental thermography including the averaged temperature in the marked black squares.

Table IV. The temperature maps obtained in simulation and by measurements are shown in Fig. 16.

Prior to the 3D thermal simulations a 3D electromagnetic (EM) simulation corresponding to the electrical operating conditions is required to obtain the power loss distribution in every finite element. This power loss distribution is directly mapped into the 3D thermal simulation as an input [29]. In this way, the high-frequency effect on the losses distribution is considered.

Furthermore, the EM equivalent properties need to be calculated and assigned in the 'Winding level FEA' simulations. To calculate these EM properties, some homogenization techniques are proposed in [20]–[23]. For the sake of simplicity, [20] is used in the corresponding EM simulations required in this section. In the AC tests shown next, two new variables are added, compared to the DC tests, which could be sources of deviation between measurements and simulations: core loss and the EM homogenization. The results for each prototype are described next.

1) **Prototype A: Inductor, P36/22, round solid copper:** In this test, the difference with measured mean temperatures of winding and core is higher than in the previous DC case. The main reason of this is the uncertainty related to the assigned EM material properties and the EM homogenization. However, it can be seen that both 'Wire level FEA' and 'Winding level FEA' have close results.

2) **Prototype B: inductor, P36/22, round litz:** The temperature rise in prototype B is lower than in prototype A for a current of similar magnitude (Table IV) due to the lower resistance of used litz bundle compared to the round solid wire. Simulation results are within the measurement error margin and close to each other (differences of 2.5 % and 1.2 % for maximum temperatures).

TABLE IV  
AC TEST CONDITIONS

Prototype	A	B	C	D	E
$T_{amb}$ [°C]	24	22	23	22	20
$f$ [kHz]	62	219	155	107	100
$I_{pk-pk}$ [A]	3.2	3.49	4.74	3.68	$pri = 3.68$ $sec = 6.64$

3) **Prototype C: inductor, PQ32/20, round litz:** By means of prototype C, the validation is carried out for a litz based winding in a highly exposed to ambient core shape with AC excitation. In this case, the maximum possible current (due to hardware limitations) is set, according to Table IV. Even with this current, the temperature rise is lower than the previous cases due to the reduced resistance of this winding. As a consequence, the relative error between measurements and errors is higher. However, in terms of absolute error, the difference is around 5°C.

4) **Prototype D: inductor, PQ32/20, foil:** The homogenization of foil winding, described in Section II-B3 is validated with AC current. Nevertheless, the same conclusion can be extracted than in Prototype D, except that the deviation of the simulation results is within the measurement error margin.

5) **Prototype E: transformer, RM8/I, round solid wire:** The last concept that needs to be validated is the homogenization applied to transformers. To do so, an RM8/I core transformer with solid copper wires of different diameters for primary and secondary windings is tested, according to Fig. 10 and Table IV. The results are shown in Fig. 21. It can be seen that the deviation between simulations and measurements is lower than 6.3 %. Furthermore, the results of both 'Wire level FEA' and 'Winding level FEA' differ in less than 5.2 %.

### C. DC and AC results summary

Regarding the previous results of the DC and AC tests, the next general conclusions can be extracted:

- Thermal measurements have an inherent error due to the discrepancy in the emissivity of the measured surfaces and the background radiation [24]–[26].
- Difference between the 3D thermal simulations using both the 'Wire level FEA' approach or the proposed 'Winding level FEA' and measurements is affected by the tolerance of the available thermal and electromagnetic material properties data provided by the manufacturers.
- In the case of the AC tests, two additional variables appear: core loss and the electromagnetic homogenization required for the 'Winding level FEA'.
- Due to the geometric modification in the 'Winding level FEA' approach, the impact of the convective heat transfer is slightly varied compared with the detailed 'Wire

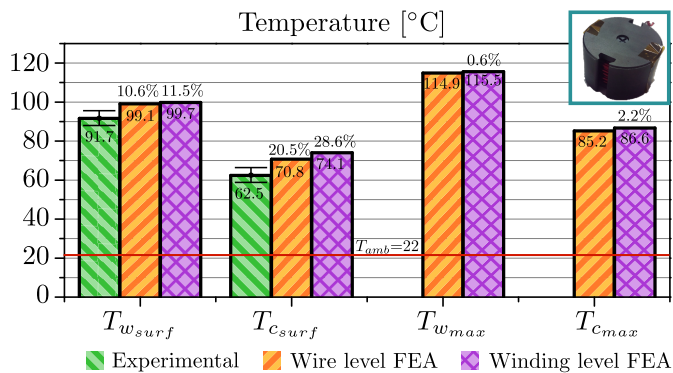


Fig. 17. AC test temperature of 'A' (P36/22 inductor, round solid wire).

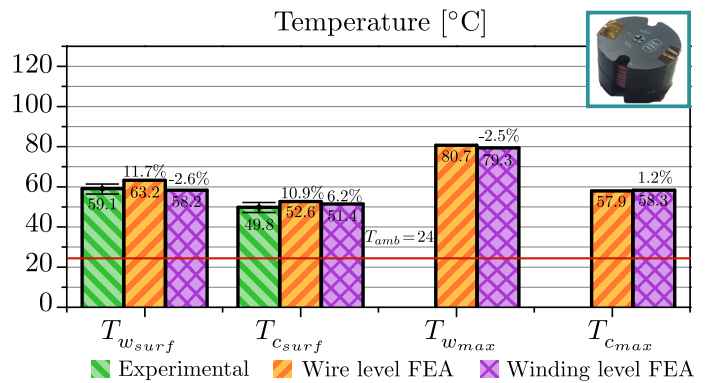


Fig. 18. AC test temperature of 'B' (P36/22 inductor, round litz bundle).

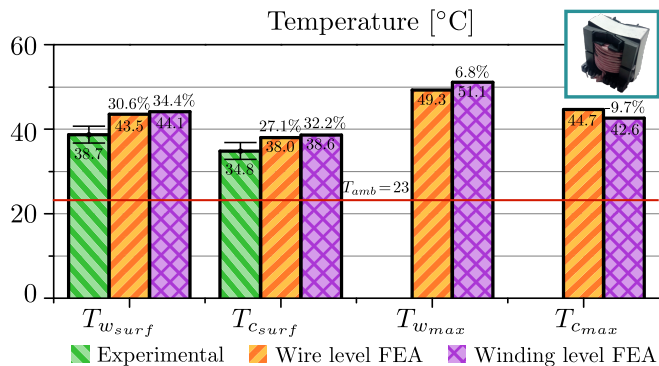


Fig. 19. AC test temperature of 'C' (PQ32/20 inductor, round litz bundle).

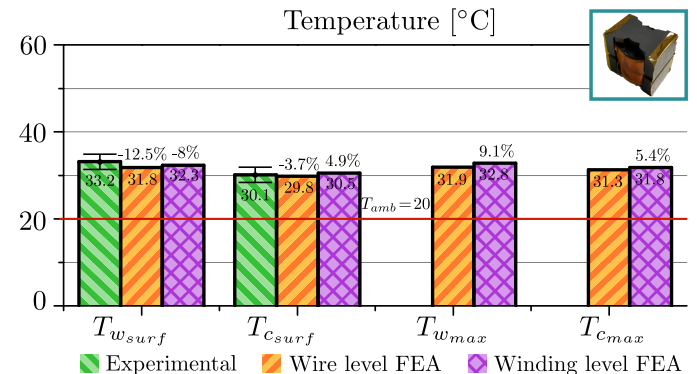


Fig. 20. AC test temperature of 'D' (PQ32/20 inductor, foil).

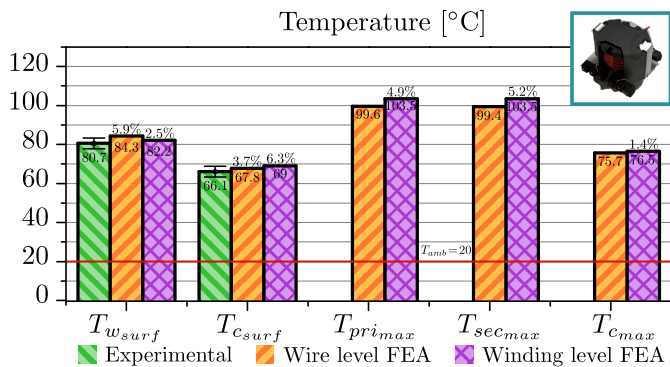


Fig. 21. AC test temperature of 'E' (RM8/I transformer, round solid wire).

level FEA'. However, the difference between each other is lower than 5°C for most cases, except for the foil inductor, where this it is lower than 9°C.

The most remarkable key point is the accuracy of the introduced two-stage thermal homogenization ('Winding level FEA') in addition to its reduced simulation time, compared with detailed simulations ('Wire level FEA'), which is analyzed next.

#### D. Finite Element Simulations: computation time

Once the accuracy of the method is analyzed, the simulation time saving due to the simpler mesh of the 'Winding level FEA' simulation is compared with the detailed 'Wire level

FEA' simulation for each prototype in Table V. It is remarkable that the 'Winding level FEA' leads to a reduction of the computation time by a factor between 6 and 8.

The results are computed with the Icepak package from ANSYS Electronics Desktop 19.1, running Intel Core i7-6700 CPU and 32 GB RAM is used. The mesh level is set as default and 100 iterations with the solve setting set to 'Flow=0.0001' and Energy to '1e-8'.

To summarize, the proposed method is validated by the previous experimental results. Furthermore, it provides almost the same performance than detailed simulations -in terms of accuracy- in addition to a much simpler mesh which leads a considerable reduction of the required simulation time.

TABLE V  
COMPUTATION TIME FOR PROTOTYPES A, B, C, D AND E WITH THE WIRE LEVEL FEA AND THE EQUIVALENT LAYER

Prototype	A	B	C	D	E
Wire level FEA	20'29"	19'25"	20'17"	10'55"	25'46"
Winding level FEA	2'55"	3'08"	2'48"	1'32"	3'11"
Reduction factor	7	6.2	7.2	7.1	8.1

#### V. CONCLUSIONS

A two-step homogenization is introduced in this paper to simplify the thermal analysis of the magnetic components used in power electronics, while keeping high accuracy. The required analytical equations and specific guidelines to model

round solid and litz wires, square litz wire and foil wound magnetics are described. Other special concerns are discussed like the modeling of transformers with interleaving and the use of insulation tape between layers.

The main advantage of this method is that it reduces the required time for 3D thermal simulations by a factor of 6–8, while keeping almost the same accuracy than more detailed simulations. Experimental prototypes (four inductors and one transformer) are built to validate this method, both with DC and AC excitation. Other contribution of this method is that convergence of 3D simulations is assured even for complex structures or litz winding, since the required mesh is much less demanding for the equivalent winding than for detailed simulations. These improvements might allow using this equivalent 3D thermal simulations within optimization processes and sensitivity analysis, thus providing more accurate temperature estimations than traditional analytical equations, leading to higher power density magnetic components.

#### ACKNOWLEDGEMENT

Guillermo Salinas holds a predoctoral contract under RD99/2011, with a grant ('Programa Propio') by the 'Universidad Politécnica de Madrid'.

#### APPENDIX A

##### DERIVATION OF THE EFFECTIVE THERMAL CONDUCTIVITY FOR FOIL WINDING

In this appendix, the derivation of the equations for the effective conductivity for rectangular and circular foil winding, used in Section II-B3, is explained.

##### A. XY rectangular winding

1) **Orthogonal effective thermal conductivity:** Considering a plane wall made by several layers of conductor material and other layers of insulator, according to Fig. 6, the total thermal resistance in the orthogonal direction (X or Y) can be calculated as the series association of the thermal resistance of each layer ([7] [8]) by means of the next expression:

$$R_{th_{ort}} = \frac{l_{cond}}{k_{cond} \cdot A} + \frac{l_{ins}}{k_{ins} \cdot A} \quad (12)$$

Being  $A$  the cross-section,  $l_{cond}$  and  $l_{ins}$  the total width of conductor and insulation regions (for Fig. 6: considering the red layers as conductors and yellow ones as insulation,  $l_{cond} = l_1 + l_3$  and  $l_{ins} = l_2 + l_4$ );  $k_{cond}$  and  $k_{ins}$  are their corresponding thermal conductivity.

Now, according to the definition of a thermal resistance,  $R_{th_{ort}}$  can be expressed in terms of its effective thermal conductivity:

$$R_{th_{ort}} = \frac{l_{tot}}{k_{eq_{ort}} \cdot A} \quad (13)$$

Rearranging this equation, the orthogonal thermal conductivity  $k_{eq_{ort}}$  can be computed as a function of the thermal conductivity and length of each material region:

$$k_{eq_{ort}} = \frac{(l_{cond} + l_{ins}) \cdot k_{cond} \cdot k_{ins}}{l_{cond} \cdot k_{ins} + l_{ins} \cdot k_{cond}} \quad (14)$$

2) **Effective thermal conductivity in the vertical direction:** Regarding the analysis of the multilayer plane wall in the vertical direction (Z), the corresponding thermal network is the parallel association of the thermal resistance of each region:

$$\begin{aligned} R_{th_z} &= \left( \frac{1}{R_{th_{cond-z}}} + \frac{1}{R_{th_{iso-z}}} \right)^{-1} = \\ &= \left( \frac{k_{cond} \cdot A_{cond}}{l_z} + \frac{k_{ins} \cdot A_{ins}}{l_z} \right)^{-1} \end{aligned} \quad (15)$$

The previous equation can be defined in terms of its effective conductivity:

$$R_{th_z} = \frac{l_z}{k_{eq_z} \cdot A_{tot_z}} \quad (16)$$

Following the same concept than in the previous case, and assuming that all regions have the same vertical length ( $l_z$ ), the effective conductivity in the vertical direction can be described as:

$$k_{eq_z} = \frac{k_{cond} \cdot A_{cond} + k_{ins} \cdot A_{ins}}{A_{cond} + A_{ins}} \quad (17)$$

##### B. RZ circular winding

In order to define the effective thermal conductivity of a circular winding, the procedure is the same than for the previous section. However, the thermal resistances in this case are expressed in cylindrical coordinates, according to Fig. 7.

1) **Effective radial thermal conductivity:** In the radial direction, the thermal resistance of each region  $n$  is defined as [7] [8]:

$$R_{th_{n-r}} = \frac{\ln(r_{n-out}/r_{n-in})}{2\pi \cdot l_z \cdot k_n} \quad (18)$$

Where  $r_{n-out}$  and  $r_{n-in}$  are the outer and inner radius of the  $n$  layer, respectively;  $l_z$  is the height of the winding; and  $k_n$  is the thermal conductivity of the  $n$  layer.

Then, analyzing the circular foil winding in the radial direction, the total radial thermal resistance is equal to the series association of each layer's thermal resistance:

$$R_{th_r} = \sum_n R_{th_{n-r}} = \frac{\ln(r_{out}/r_{in})}{2\pi \cdot l_z \cdot k_{eq_r}} \quad (19)$$

Where  $r_{out}$  and  $r_{in}$  are the outer and inner radius of the whole winding and  $k_{eq_r}$  is the effective thermal conductivity in the radial direction.

Finally, by rearranging the previous equation,  $k_{eq_r}$  can be described in terms of the radius and conductivity of each layer:

$$k_{eq_r} = \frac{\ln(r_n/r_1) \cdot k_{cond} \cdot k_{ins}}{k_{ins} \sum_{n_{cond}} \ln\left(\frac{r_{n+1}}{r_n}\right) + k_{cond} \sum_{n_{ins}} \ln\left(\frac{r_{n+1}}{r_n}\right)} \quad (20)$$

2) **Effective thermal conductivity in the vertical direction:** In both rectangular and circular foil winding cases, (17) is applied.

## REFERENCES

- [1] *Ferrites and accessories*, TDK, Appl. Note, May 2017.
- [2] *Powder Cores catalog*, Magnetics Inc., 2017.
- [3] L. M. Escribano, P. Zumel, R. Prieto, J. A. Oliver, and J. A. Cobos, "A very simple analytical approach of thermal modeling for magnetic components," in *Applied Power Electronics Conference and Exposition, 2005. APEC 2005. Twentieth Annual IEEE*, vol. 3. IEEE, 2005, pp. 1944–1950.
- [4] M. Delhommais, J. Schanen, F. Wurtz, C. Rigaud, C. S., and S. Vighetti, "Thermal model of litz wire toroidal inductor based on experimental measurements," in *Applied Power Electronics Conference and Exposition, 2018. APEC IEEE*. IEEE, 2018, pp. 2658–2665.
- [5] J. C. Fagundes, A. J. Batista, and P. Viarouge, "Thermal modeling of pot core magnetic components used in high frequency static converters," *IEEE Transactions on magnetics*, vol. 33, no. 2, pp. 1710–1713, 1997.
- [6] L. M. Escribano, R. Prieto, J. A. Oliver, J. A. Cobos, and J. Uceda, "Analytical thermal model for magnetic components," in *Power Electronics Specialist Conference, 2003. PESC'03. 2003 IEEE 34th Annual*, vol. 2. IEEE, 2003, pp. 861–866.
- [7] T. L. Bergman, A. S. Lavine, F. P. Incropera, and D. P. Dewitt, *Fundamentals of heat and mass transfer*, 7th ed. John Wiley & Sons New York, 2012.
- [8] Y. Cengel, *Heat and mass transfer: fundamentals and applications*. McGraw-Hill Higher Education, 2014.
- [9] K. Pietrak and T. S. Wisniewski, "A review of models for effective thermal conductivity of composite materials," *Journal of Power Technologies*, vol. 95, no. 1, p. 14, 2015.
- [10] F. Chauvicourt, P. Romanazzi, D. Howey, A. Dziechciarz, C. Martis, and C. T. Faria, "Review of multidisciplinary homogenization techniques applied to electric machines," in *Ecological Vehicles and Renewable Energies (EVER), 2016 Eleventh International Conference on*. IEEE, 2016, pp. 1–9.
- [11] G. Salinas, A. Delgado, J. A. Oliver, and R. Prieto, "Fast FEA thermal simulation of magnetic components by winding equivalent layers," in *Energy Conversion Congress and Exposition (ECCE), 2018 IEEE*. IEEE, 2017, pp. 1–120.
- [12] *Materials catalog*, Available: <http://www.goodfellow.com/E/Copper.html> [Accessed: 17 - Dic - 2018], Goodfellow - Supplier of materials for research and development, 2018.
- [13] L. Siesing, A. Reinap, and M. Andersson, "Thermal properties on high fill factor electrical windings: Infiltrated vs non infiltrated," in *Electrical Machines (ICEM), 2014 International Conference on*. IEEE, 2014, pp. 2218–2223.
- [14] Z. Hashin and S. Shtrikman, "A variational approach to the theory of the elastic behaviour of multiphase materials," *Journal of the Mechanics and Physics of Solids*, vol. 11, no. 2, pp. 127–140, 1963.
- [15] N. Simpson, R. Wrobel, and P. H. Mellor, "Estimation of equivalent thermal parameters of impregnated electrical windings," *IEEE Transactions on Industry Applications*, vol. 49, no. 6, pp. 2505–2515, 2013.
- [16] M. Jaritz, A. Hillers, and J. Biela, "General analytical model for the thermal resistance of windings made of solid or litz wire," *IEEE Transactions on Power Electronics*, 2019.
- [17] P. A. Kyaw, J. Qiu, and C. R. Sullivan, "Analytical thermal model for inductor and transformer windings and litz wire," in *2018 IEEE 19th Workshop on Control and Modeling for Power Electronics (COMPEL)*. IEEE, 2018, pp. 1–9.
- [18] R. Wrobel, S. Ayat, and J. L. Baker, "Analytical methods for estimating equivalent thermal conductivity in impregnated electrical windings formed using litz wire," in *Electric Machines and Drives Conference (IEMDC), 2017 IEEE International*. IEEE, 2017, pp. 1–8.
- [19] C. R. Sullivan, "Prospects for advances in power magnetics," in *CIPS 2016: 9th International Conference on Integrated Power Electronics Systems; Proceedings of*. VDE, 2016, pp. 1–9.
- [20] X. Nan and C. R. Sullivan, "An equivalent complex permeability model for litz-wire windings," *IEEE Transactions on Industry Applications*, vol. 45, no. 2, pp. 854–860, 2009.
- [21] R. Y. Zhang, J. K. White, J. G. Kassakian, and C. R. Sullivan, "Realistic litz wire characterization using fast numerical simulations," in *2014 IEEE Applied Power Electronics Conference and Exposition-APEC 2014*. IEEE, 2014, pp. 738–745.
- [22] A. Roßkopf, E. Bär, C. Joffe, and C. Bonse, "Calculation of power losses in litz wire systems by coupling fem and peec method," *IEEE Transactions on Power Electronics*, vol. 31, no. 9, pp. 6442–6449, 2016.
- [23] A. Delgado, G. Salinas, J. A. Oliver, J. A. Cobos, J. Rodríguez, and S. Premo, "Equivalent parameters of round and litz wire conductors to obtain an equivalent layer to accelerate finite element simulations of wireless power transfer system," in *2018 IEEE Energy Conversion Congress and Exposition (ECCE)*. IEEE, 2018, pp. 7375–7379.
- [24] *Thermal Imaging Guidebook for Industrial Applications*, FLIR, Appl. Note, 2011.
- [25] *Thermal Imaging cameras: a fast and reliable tool for testing solar panels*, FLIR, Technical Note, 2007.
- [26] *Ti200, Ti300, Ti400 - Thermal Imagers*, FLUKE, User Manual, 2013.
- [27] *Ferrite materials survey*, Ferroxcube, 2008.
- [28] The engineering toolbox: Air - thermal conductivity. [Online]. Available: [https://www.engineeringtoolbox.com/air-properties-viscosity-conductivity-heat-capacity-d\\_1509.html](https://www.engineeringtoolbox.com/air-properties-viscosity-conductivity-heat-capacity-d_1509.html) [Accessed 01-12-2018]
- [29] *Icepak Help Release 2019 R1*, ANSYS Inc., January 2019.



**Guillermo Salinas** received the B.Sc. degree in electronics engineering from the 'Universidad Miguel Hernández', Spain, and the M.Sc. degree in industrial electronics from the 'Universidad Politécnica de Madrid' (UPM), Spain, in 2015 and 2016 respectively. In both universities he has been enrolled in the corresponding power electronics research centers from 2014 to the present, participating on the design and optimization of power converters for space applications and other R&D projects for important companies of the sector.

His current PhD research interests are focused on the thermal modeling of high-frequency magnetic components and its optimization. He made his doctoral stay at the European Space Agency. ORCID: 0000-0002-7065-0995



**Alberto Delgado** received the B.Sc. degree in Electrical Engineering at the University of Málaga (UMA), Spain, in 2016. During his undergraduate studies, he was awarded honors on several occasions and he achieved the Best Student of the Year Award. Furthermore, he received the M.Sc. degree in Industrial Electronics at the Universidad Politécnica de Madrid (UPM) in 2017. He is currently working towards a Ph.D. degree in Industrial Electronics at UPM.

His research activities include modelling of dc converters for Inductive Power Transfer system, magnetic components for different applications such as RFID communications and wireless charging; and magnetic nano-materials and micro-materials. ORCID: 0000-0002-7099-6961



**Javier Muñoz-Antón** received the Master and Doctoral degrees on Mechanical Engineering from Universidad Politécnica de Madrid (UPM), Spain, in 2005 and 2008 respectively. He became Assistant Professor in 2006 and Associate Professor in 2012. He has been author and co-author in more than 90 scientific paper on Journals and Conferences and he holds 30 patents. His research interests include heat transfer, thermal engineering, thermal inefficiencies, thermal modelling, CFD, cryogenics and renewable energy.

Dr. Javier Muñoz-Antón has led several research projects with private and public funding, and he has participated in more than 20 direct R&D projects with companies in Europe. ORCID: 0000-0002-1980-0863



**Jesús A. Oliver** received the Master and Doctoral degrees in Electrical Engineering from Universidad Politécnica de Madrid (UPM), Spain, in 1996 and 2007 respectively. He became Assistant Professor in 2001 and Associate Professor at UPM in 2007. He has been author and co-author in more than 150 scientific papers on Journals and Conferences and he holds 5 patents. His research activities include modelling (dc-dc converters, magnetic components, piezoelectric transformers, fuel-cells, and DC distributed power electronic systems), fast control techniques for dc-dc converters for VRM applications and RF amplifiers, three-phase rectifiers for aircraft applications, wireless power transfer and power systems on Chip.

Dr. Jesús A. Oliver has led numerous research projects with private and public funding, and he has participated in more than 50 direct R&D projects with companies in Europe, US, Australia and China. Currently he is serving as Associate Editor of the IEEE Transactions on Power Electronics. ORCID: 0000-0002-5286-5378



**Roberto Prieto** received the master's and Doctoral degrees in electrical engineering from the Universidad Politécnica de Madrid, Spain, in 1993 and 1998, respectively.

He is a Full Professor with Universidad Politécnica de Madrid. His contributions are focused in the field of power supply systems for telecom, aerospace, automotive, and medical applications. His research interests include magnetic components, modeling, power electronics CAD tools, and modeling of components and systems for power delivery.

He has published over 250 technical papers and holds two patents. He has been actively involved in over 50 research and development projects awarded with public funding in competitive programs, and above 40 direct contracts for research and development for different companies worldwide, including ANSYS, Alcatel, Intel, General Electric, Indra, Siemens, Philips, EADS, and Boeing and Sener. Prof. Prieto was a recipient of the UPM Researcher Award for faculty younger than 35 years of age. He has advised six Doctoral dissertations and conducted several professional seminars and tutorials. ORCID: 0000-0001-7361-6816